RESEARCH ARTICLE

Diazaborines are a Versatile Platform to Develop ROS-Responsive Antibody Drug Conjugates

João P. M. António,[a]‡ Joana Inês Carvalho, [a]‡ Ana S. André, [b] Joana N. R. Dias, [b] Sandra I. Aguiar, [b] Hélio Faustino,[a] Ricardo M. R. M. Lopes,[a] Luis F. Veiros,[c] Gonçalo J. L. Bernardes,[d] [e] Frederico A. da Silva,[b] Pedro M. P. Gois [a]*.

[a] Dr. J. P. M. António, J. I. Carvalho, Dr. H. Faustino, R. M. R. M. Lopes, Dr. Pedro M. P. Gois
Research Institute for Medicines (iMed.ULisboa)
Faculdade de Farmácia, Universidade de Lisboa, Lisboa, Portugal
Av. Prof. Gama Pinto,1649-003 Lisboa, Portugal
E-mail: pedrogois@ff.ul.pt

[b] A. S. André, Dr. J. N. R. Dias, Dr. S. I. Aguiar, Dr. F. A. da Silva
Centro de Investigação Interdisciplinar em Sanidade Animal
Faculdade de Medicina Veterinária, Universidade de Lisboa, Lisboa, Portugal
Av. Universidade Técnica, 1300-477 Lisboa, Portugal
E-mail: fasilva@fmv.ulisboa.pt

[c] Dr. L. F. Veiros
Centro de Química Estrutural and Departamento de Engenharia Química
Instituto Superior Técnico, Universidade de Lisboa, Portugal
Av. Rovisco Pais 1, 1049-001 Lisboa, Portugal
E-mail: veiros@tecnico.ulisboa.pt

[d] Dr. G. J. L. Bernardes
Instituto de Medicina Molecular João Lobo Antunes,
Faculdade de Medicina, Universidade de Lisboa
Avenida Professor Egas Moniz, 1649-028 Lisboa, Portugal.
E-mail: gbernardes@medicina.ulisboa.pt

[e] Dr. G. J. L. Bernardes
Yusuf Hamied Department of Chemistry
University of Cambridge
Lensfield Road, CB2 1EW, Cambridge, United Kingdom
E-mail: gbernardes@medicina.ulisboa.pt

‡These authors contributed equally to the work.

Abstract: Antibody-drug conjugates (ADCs) are a new class of therapeutics that combine the lethality of potent cytotoxic drugs with the targeting ability of antibodies to selectively deliver drugs to cancer cells. The synthesis of ADCs is challenging, and studies in this area show that their therapeutic effect is highly dependent on the chemistries used to connect both functions. Therefore, the linker evolved in recent years from being a simple chemical spacer to a functional structure that controls the potency and selectivity of ADCs. The linker provides a platform to integrate mechanisms to access synthetic homogeneity, stability in circulation and more importantly, the installation of chemical units that release the drug as a response to the disease's chemical environment. In this study we show for the first time the synthesis of a reactive-oxygen-species (ROS) responsive ADC (VL-DAB31-SN-38) that is highly selective and cytotoxic to B-cell lymphoma (CLBL-1 cell line, IC_{50} value of 54.1 nM). The synthesis of this ADC was possible due to the discovery that diazaborines (DABs) are a very effective ROS-responsive unit (0.422 and 0.103 $M^{-1}s^{-1}$ with 100 and 10 equiv of H_2O_2 respectively), that is also very stable in buffer (over 14 days at different pHs) and in plasma (over 5 days). DFT calculations performed on this system revealed a favorable energetic profile (ΔGR = –74.3 kcal/mol) similar to the oxidation mechanism of aromatic boronic acids. DABs' very fast formation rate and modularity enabled the construction of different ROS responsive linkers featuring self-immolative modules, bioorthogonal functions and bioconjugation handles. These structures were used in the site-selective functionalization of a VL antibody domain and in the construction of the homogeneous ADC. The enclosed ROS-responsive linker technology based on DABs is expected to become a valuable tool to prepare stimuli-responsive therapeutic materials, as ROS is a very important hallmark in several important diseases.

Introduction

Antibody-drug conjugates (ADCs) have emerged as a promising therapeutic class for cancer treatment due to its enhanced toxicological profile and selectivity.[1] These biopharmaceutical drugs consist of monoclonal antibodies (mAb) connected to a cytotoxic drug via a cleavable or non-cleavable linker and, currently, there are eleven ADCs approved for clinical usage. ADCs design has evolved to more homogeneous constructs with better pharmacokinetics properties and responsive linkers, which allow a controlled release of active payloads inside cancer cells[2] These linkers employ chemistries triggered by a specific stimulus that enhances drug release in cancer cells, conferring a functional character to cleavable linkers and improving overall antitumor performance.[3] Nevertheless, cleavable linkers are more prone to fail due to instability in circulation and off-target toxicity. Seeking more robust linker technologies that can still be triggered by enzymatic or chemical features in the precise targeted cells, remains a challenge in ADC development.[1]

In recent years, reactive oxygen species (ROS) gained considerable recognition because of their central role in cellular homeostasis through the regulation of numerous signaling pathways.[4] This family of signaling molecules is responsible for, among others mechanisms, controlling DNA transcription and

regulating cell proliferation and differentiation. The vast majority of cellular ROS (≈ 80%) is generated during the oxidative phosphorylation in the electron transport chain of mitochondria, with the remaining part being produced in peroxisomes and endoplasmic reticulum.[5] In high levels, ROS are harmful to cells as they can damage proteins, lipids and DNA, ultimately leading to metabolic disfunction and cell death.[6] Thus, cells have built-in mechanisms to counterbalance the increase of ROS levels which include a complex scavenging system based on glutathione (GSH) and redox enzymes such as superoxide dismutase, glutathione peroxidase, glutathione reductase, thioredoxin and catalase.[6–8] The preservation of this tenuous redox balance is essential for maintaining cellular homeostasis.

Contrary to healthy cells, cancer cells, due to a defective mitochondrial oxidative metabolism, have an inherently high level of ROS which is indispensable to sustain the biochemical alterations required for the initiation, promotion and progression of the disease.[9] The elevated oxidative stress in cancer cells, when compared with healthy cells, has been explored as a trigger to promote the selective delivery of cytotoxic and imaging payloads.[10–12] These drug delivery systems are generally based on nanoparticles and polymeric supramolecular constructs bearing organochalcogen, thioether, thioketal or aryloxalate linkages that, when exposed to ROS, promote the payload release upon changing their physical properties.[10] Interestingly, although this strategy has been used to successfully promote the drug delivery of different nanosystems, to the best of our knowledge, these linkages have not been used in the construction of well-defined ROS-responsive targeting drug conjugates like ADCs. This lack of use is probably related with the fact that these functions endure the physiologic conditions more effectively when incorporated in a material's supramolecular structure rather than when solvent exposed in the form of a bioconjugate linker. Therefore, the engineering of innovative architectures of well-defined ROS-responsive targeting drug conjugates relies on the discovery of chemical functions that sense disease-associated concentrations of ROS, while maintaining the structural integrity of the bioconjugate in circulation.

Aromatic boronic acids (BAs) are well-known for being readily oxidized to the corresponding phenols in the presence of various ROS, and this unique mechanism has been extensively explored in the design of multiple functional materials for drug delivery (Fig. 1a).[13,14] However, aromatic BAs also exhibit poor stability under physiologic conditions and a promiscuous reactivity with endogenous molecules, such as vicinal diols or proteins, which often translates into poor pharmacokinetic and toxicity profiles.[15,16] Therefore, despite very favorable oxidation kinetics in the presence of ROS, the instability and off-target reactivity of BAs constitute a major obstacle for the use of this function in the design of ROS-responsive linkers for targeted drug conjugates.

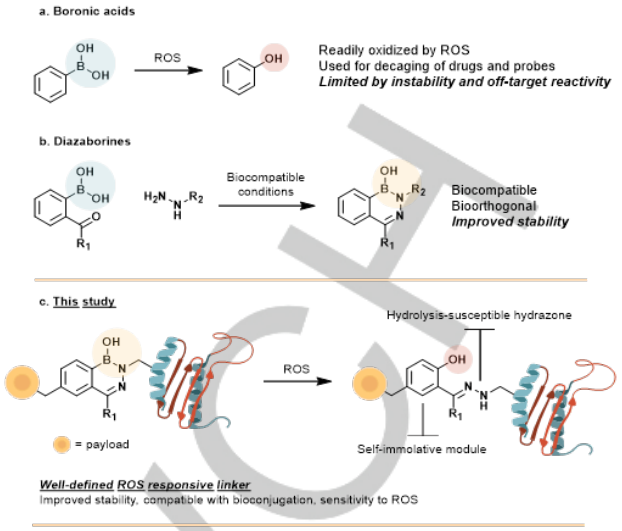

Figure 1. Proposed structure for ROS-responsive linker based on DAB scaffold. **(a)** Aromatic boronic acids oxidation by ROS; **(b)** Diazaborines as bioorthogonal bioconjugation tool; **(c)** This study: Diazaborines oxidation by ROS and its application as ROS-responsive linkers for targeting drug conjugates. ROS, reactive species of oxygen.

In the early 80s, diazaborines (DABs) emerged as a promising class of boronated heterocycles with antibacterial properties.[17–20] More recently, the very efficient formation of DABs under bioconjugation conditions, established this reaction as a powerful click-type transformation in chemical biology.[21,22] In DABs, the BA function is inserted in a B–N heterocycle where the boron vacant orbital is stabilized by the lone pair of electrons of the adjacent nitrogen (Fig. 1b).[15,19,23] Despite this, as corroborated by recent studies, this architecture does not suppress the Lewis acidity of the boron center.[24] Therefore, we envisioned that, if DAB's boron center retains the BA's oxidative sensitivity in the presence ROS, the improved stability of this scaffold could contribute to bridge the technological gap that limits the construction of well-defined ROS-responsive linker for targeting drug conjugates. The demonstration of this hypothesis constitutes the main focus of this study (Fig. 1c).

Results and Discussion

Depending on the stereo-electronic properties of the hydrazine and 2-carbonylphenyl BA components, DABs with different stabilities under aqueous media can be obtained as a consequence of the equilibrium between the close and the open forms.[20] In the open form, the BA function is exposed and the hydrazone linkage is expected to be more prone to hydrolysis. Therefore, we initiated this study by evaluating the influence of different substituents in the formation and stability of these heterocycles. Hence a panel of DABs was synthesized by mixing in water 2-formylphenyl BA (2-FPBA) or 2-acetyl phenyl BA (2-APBA) with hydrazines featuring different N-substituents (Fig. 2a).

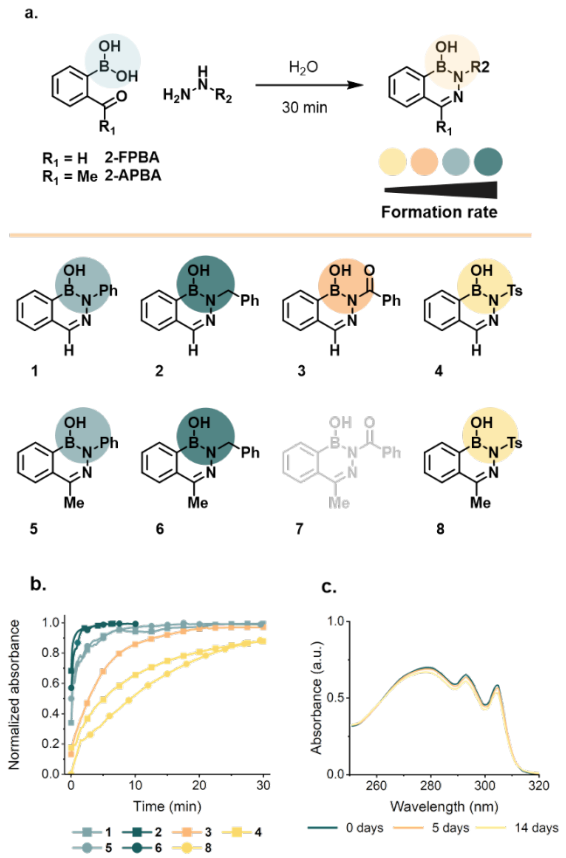

Figure 2. Diazaborines **1-8** and their stability in ammonium acetate 20 mM pH 7.4 at 25°C. **(a)** Diazaborines prepared from the reaction of phenyl, benzyl, benzoyl and tosyl hydrazines with 2-FPBA and 2-ABPA; **(b)** Normalized formation kinetics of DABs **1-8** (**7** was excluded due to unreliable results); **(c)** UV-Vis spectra of compound **2** after 5 and 14 days stability in ammonium acetate 20 mM pH 7.4 at 25°C.

Once prepared, DABs **1-8** were tested for their stability in ammonium acetate pH 7.4 at 25°C. As shown in previous studies, also in this assay, DABs **2-4**, prepared from 2-FPBA proved to be considerably more stable than those prepared from 2-APBA (**5-8**), as no degradation was observed for these compounds over 14 days (Fig. 2c and Supplementary Fig. S5). Despite being prepared from 2-FBPA, compound **1** displayed a poor stability which is possibly related with the low stability of the phenyl hydrazine in these conditions.

The reaction of hydrazines with 2-carbonylphenyl BA was shown to exhibit very fast kinetics and have been used recently as a click-type reaction to assemble bioconjugates.[22,25] Therefore, we studied the formation kinetics of DABs **1-8** (**7** was excluded from this study due to unreliable results possibly related to possibly due to the already reported equilibrium of open and closed forms and the formation of dimers).[26] As shown in Fig. 2b, in ammonium acetate pH 7.4 (final concentration 60 μM), the reaction of benzyl hydrazine with 2-FPBA and 2-ABPA displayed the fastest kinetics, generating DABs **2** and **6** in less than 10 min, while hydrazines with electron withdrawing *N*-substituents were slightly slower, affording the respective DABs in up to 1h. Interestingly, pairs bearing the same *N*-substituent appear to display similar reaction rates, implying that the stereo-electronic properties of the hydrazine substituent are essential to the reaction kinetics.

Considering these results, DABs featuring alkylic *N*-substituents like DAB **2** and **6** displayed the best performance in terms of stability in aqueous conditions and kinetics of formation. Therefore, we next tested if DABs retained the ability to be oxidized in the presence of ROS. Hence, a 50 μM solution of **2** was incubated with 100 equiv of H_2O_2 (ammonium acetate 20 mM pH 7.4). After 30 min, the mixture was analyzed by Electrospray Ionization-Mass Spectrometry (ESI-MS) and DAB **2** generated the corresponding salicyl-hydrazone **9** (Fig. 3). Similar oxidations were observed for the remaining DABs **1-8** under these conditions (Supplementary Fig. S8).

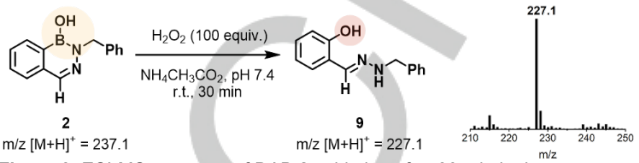

Figure 3. ESI-MS spectrum of DAB **2** oxidation after 30 min in the presence of 100 equiv of H_2O_2 peroxide. Compound **2** (10 mM, DMF) was diluted in ammonium acetate solution 20 mM at pH 7.4 to a final concentration of 50 μM in the presence of 100 equiv of H_2O_2. The mixture was stirred at 25ºC for 30 min and then analysed by ESI-MS to observe the full conversion into the corresponding salicyl-hydrazone **9**.

Encouraged by these results, the aqueous stability of DAB **2** was further tested in more demanding conditions, namely at different pHs and in human plasma. Hence, DAB **2** (100 μM) was incubated in at pH 4.5 (acetate buffer 50 mM), 7.4 (KPi buffer 50 mM) and 9.0 (carbonate buffer 50 mM) at 25°C and the stability was monitored by High Performance Liquid Chromatography (HPLC) at different time points. As shown in Fig. 4a, DABs concentration remained constant after 14 days in all three conditions. Similar results were obtained upon incubation of DAB **2** in human plasma at 37ºC (120 μM), with no visible degradation after 5 days.

Pleased with its stability, we decided to study the oxidation process in detail. We incubated DAB **2** with 100 equiv of H_2O_2 at pH 7.4 (ammonium acetate 20 mM) and followed the disappearance of the starting material by HPLC. As observed in Fig. 4b, at 100 μM the starting material was swiftly oxidized, with a calculated oxidation half-life around 15 min. Proportional results were obtained when repeating the experiment with 50 μM, 500 μM and 1 mM of starting material which enabled the determination of the reaction rate as 0.422 M^{-1} s^{-1} (Supplementary Fig. S9 and S11).

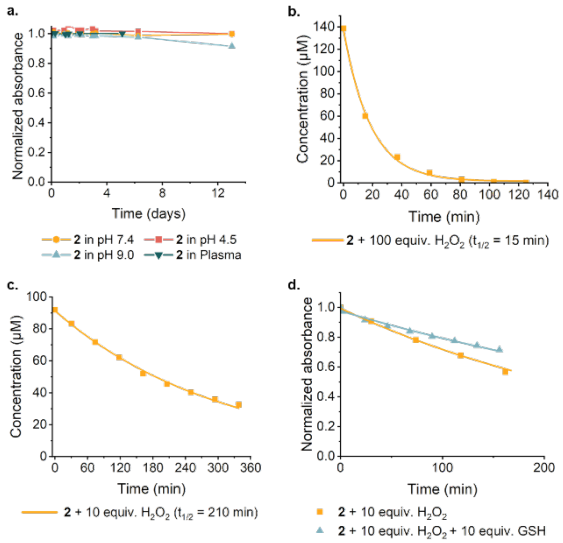

Figure 4. Stability of DAB **2** at different conditions. **(a)** Stability of DAB **2** at pH 4.5, 7.4, 9.0 at 25°C and in plasma at 37°C; **(b)** Oxidation profile of DAB **2** (pH

7.4, 25ºC) in the presence of 100 equiv H_2O_2; and **(c)** 10 equiv H_2O_2; **(d)** Oxidation profile of DAB **2** (pH 7.4, 25°C) in the presence and absence of glutathione. DAB, diazaborine; GSH, glutathione.

Although ROS plays a fundamental role in tumoral proliferation, the increased intracellular concentration of ROS can be noxious for tumor cells if not adequately counterbalanced. The major redox balancing mechanism in tumor cells encompasses an increase in GSH concentration and this delicate equilibrium is essential to maintain the redox homeostasis of cancer cells. Therefore, we questioned if H_2O_2 would still be able to oxidize DABs in the presence of high concentrations of GSH. To simulate cancer cell conditions, DAB **2** (100 μM) was incubated with 10 equiv of GSH (1 mM), followed by the addition of 10 equiv of H_2O_2 (1 mM). As expected, although the reaction in the presence of GSH is slightly slower (Fig. 4d), importantly, the oxidation mechanism is still operative.

Next, we investigated the influence of the pH in the oxidation rate. Accordingly, DAB **2** (100 μM) was incubated with 100 and 10 equiv of H_2O_2 in carbonate buffer 50 mM at pH 9.0. Under these conditions the oxidation was clearly accelerated, proceeding with half-lives of 5 and 14 min, respectively (Fig. 5a-b). Inversely, when the assay was performed in acetate buffer 50 mM at pH 4.5, the oxidation was completely inhibited, even in the presence of 100 equiv of oxidizing agent (Fig. 5c-d).

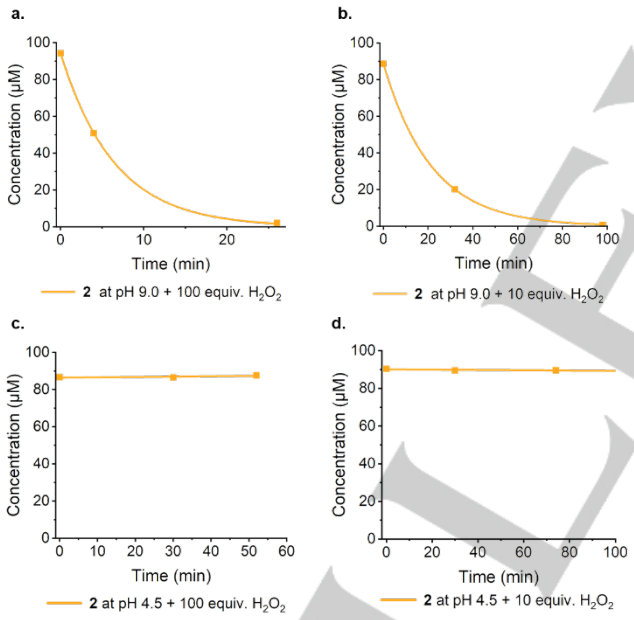

Figure 5. Oxidation profile of DAB **2** at pH 9.0 or 4.5 at 25°C. At pH 9 in the presence of **(a)** 100 equiv and **(b)** 10 equiv H_2O_2; At pH 4.5 in the presence of **(c)** 100 equiv and **(d)** 10 equiv H_2O_2.

To rationalize some of the aforementioned observations, we studied the oxidation mechanism of DAB **2** in the presence of H_2O_2 by means of DFT calculations.[27] The result is depicted in a simplified way in Fig. 6, showing the more relevant steps along the path. The detailed profile is presented as Supporting Information (Supplementary Fig. S43).

The mechanism starts with nucleophilic attack of the peroxide O-atom to the boron atom of the DAB molecule, overcoming a barrier of 23.1 kcal/mol. The next relevant step is the aryl transposition from the boron to the O-atom with an associated barrier of $\Delta G^{\ddagger}$ = 28.2 kcal/mol. This is the highest barrier of the entire mechanism (**TS_{CD}**) and corresponds to the overall energy barrier of the reaction. The path proceeds with nucleophilic attack of a water molecule and B–N bond breaking and, finally, there is hydrolysis of the O–B bond by a second water molecule, producing the final phenol group and boric acid. The reaction is thermodynamically favorable with an overall free energy balance of ΔG_R = –74.3 kcal/mol. The mechanism calculated allows a rationalization of the observed pH influence on the reaction rate. Accordingly, under acidic conditions the H_2O_2 will be mostly protonated and, consequently, unable to attack the boron, whereas in basic medium its nucleophilicity is increased, facilitating the attack that is the starting point of the reaction.[28,29] The equivalent mechanism with phenyl BA as substrate, was also calculated for comparison purposes (Supplementary Fig. S44). These results indicate a slightly more facile reaction than the one involving DAB **2**, with a lower overall barrier ($\Delta G^{\ddagger}$ = 26.1 kcal/mol) as well as a more favorable free energy balance (ΔG_R = –91.9 kcal/mol). However, the difference is quite small and clearly support the observed oxidation of DABs.

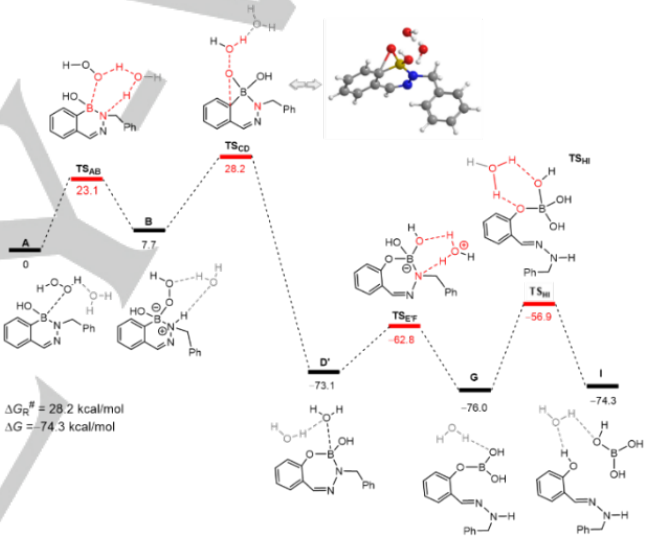

Figure 6. Simplified free energy profile calculated for the oxidation of DAB **2** by H_2O_2 (most relevant steps). Free energy values (kcal/mol) relative to the initial reactants **A**. DFT calculations at the M06-2X/6-311G(d,p) level were performed using the GAUSSIAN 09 package. The model used in the calculations included an explicit water molecule and solvent effects (water) were further considered by means of the PCM model. A complete account of the computational details and the corresponding list of references are provided as SI.

Once established that alkylic-derived DABs are a valuable scaffold to design ROS-responsive linkers, we initiated a study to integrate this responsive moiety in the structure of a functional bioconjugate. Considering that, upon DAB oxidation a hydrolysis-susceptive hydrazone is generated, we first designed a linker in which the biomolecule is attached to the 2-FPBA component through a maleimide, while the functional payload is linked to the hydrazine. Therefore, the 2-FPBA was modified to install a maleimide function over 6 synthetic steps starting from **10** (Fig. 7a and Supporting Information). Once prepared, cross-linker **11** was reacted with benzyl hydrazine to generate DAB **12**, which was evaluated in the functionalization of a model peptide featuring a cysteine (Cys) residue. As shown in Fig. 7, the bioconjugation with laminin fragment effectively afforded bioconjugate **13** which was successfully oxidized with H_2O_2 overnight (Fig. 7b-c).

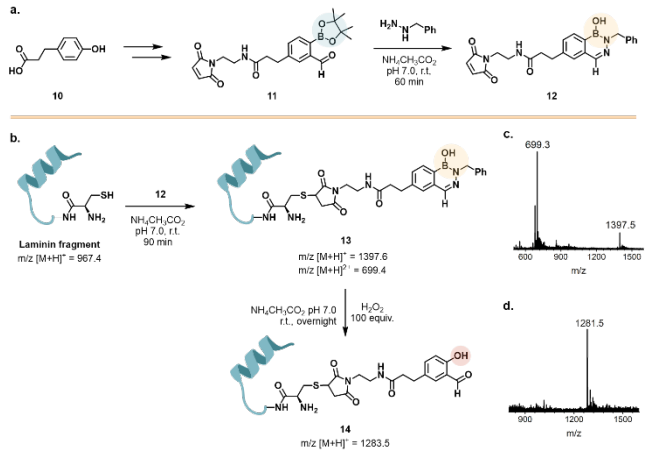

Figure 7. Bioconjugation reaction between DAB **12** and Laminin fragment. **(a)** Model DAB **12**, synthesized from **11** and benzyl hydrazine; **(b)** schematic representation of the conjugation between laminin and DAB **12** followed by oxidation with H_2O_2; **(c)** ESI-MS after bioconjugation; **(d)** ESI-MS in the presence of 100 equiv H_2O_2 overnight.

As shown in Fig. 7, the oxidation process also promoted the hydrolysis of the hydrazone. Based on this observation, we envisioned the possibility of exploiting this hydrolysis to trigger the release of a payload through a self-immolative mechanism. With this objective in mind, the strategies depicted in Fig. 8 were delineated to study if either the hydrazone or the salicylaldehyde components could act as self-immolative modules. Considering the results previously obtained in Fig. 7, we first evaluated route A (Fig. 9). Hence, DABs **15** and **16** featuring a model benzyl alcohol were synthesized and evaluated in terms of stability (KPi 50 mM, pH 7.4) and oxidation (100 equiv. H_2O_2, KPi 50 mM, pH 7.4). Interestingly, DAB **15** proved to be quite unstable even in the absence of hydrogen peroxide, favoring the elimination of benzyl acrylate **18**. On the other hand, DAB **16** was tested in the same conditions and exhibited a half-life of 9.2 days in KPi buffer at pH 7.4. More importantly, in the presence of H_2O_2, DAB **16** was readily oxidized (80 min half-life) to generate salicylaldehyde **19**, the hydrazone **20** and benzyl alcohol **21**. Analyzing the evolution of the oxidation reaction (Fig. 9), upon addition of the oxidant, the concentration of salicyl hydrazone **19** rapidly increases, followed by a second stage characterized by a slow decrease in concentration of **19** (Fig. 9c). This kinetics profile suggests the oxidation step is faster than the hydrazone's hydrolysis to release benzyl alcohol **21.**

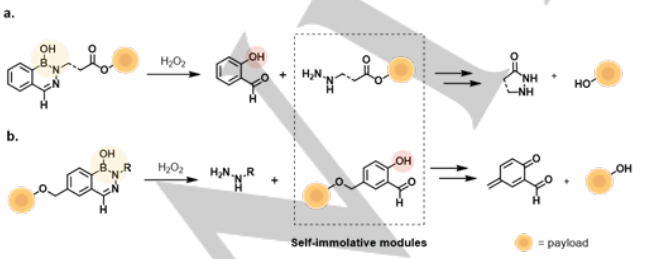

Figure 8. Two strategies to design a triggered self-immolative release of a payload. The self-immolative module is incorporated **(a)** on the hydrazine moiety or **(b)** in the boronic acid/phenol module.

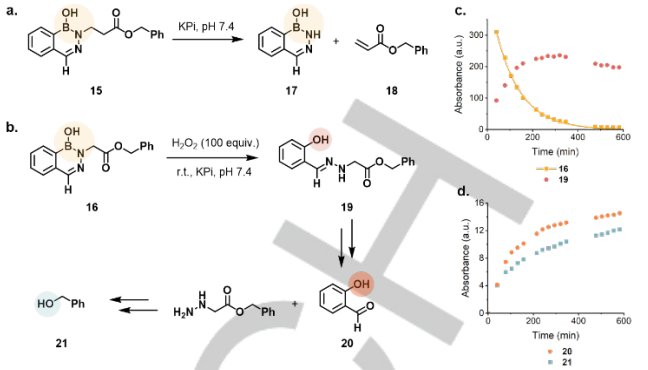

Figure 9. DABs **15** and **16** featuring a model benzyl alcohol - stability and oxidation. **(a)** DAB **15** was shown to be unstable at pH 7.4; **(b)** DAB **16** is oxidized in the presence of 100 equiv H_2O_2 and the hydrazine formed promotes the release of benzyl alcohol **21**; **(c)** HPLC profiles (pH 7.4, 25°C) of DAB **16** and the intermediate salicyl hydrazone **19** after incubation with 100 equiv H_2O_2; **(d)** HPLC profiles (pH 7.4, 25°C) of salicyl aldehyde **20** and benzyl alcohol **21** after incubation of DAB **16** with 100 equiv H_2O_2.

Based on these results we next addressed the functionalization of the linker with the cytotoxic payload SN-38, a widely used cytotoxic agent in the clinic. Recently, SN-38 was used in the construction of an antibody drug conjugate (ADC - Sacituzumab govitecan - Trodelvy®) that was approved by FDA for the treatment of triple negative breast cancer.[30–33] In our design, SN-38 was functionalized with the linker at the hydroxyl adjacent to the lactone ring, resulting in a esterification that generates a more stable construct.

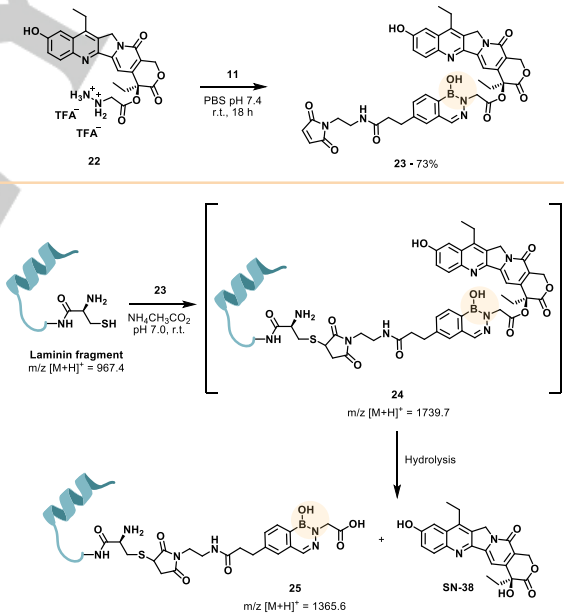

Figure 10. Synthetic route for the preparation of linker-payload **23** and its use in the modification of a laminin fragment. The bioconjugation reaction was analysed by ESI-MS to confirm the presence of bioconjugate **24** and hydrolyzed conjugate **25** in small amounts. TFA, trifluoroacetic acid.

As shown in Fig. 10, compound **22** was reacted with the 2-FPBA component **11** to yield the DAB **23** that was used in the functionalization of the laminin fragment peptide. The bioconjugation reaction produced mainly bioconjugate **24**, though careful analysis of the ESI-MS spectra indicated that the hydrolyzed conjugate was also being produced in small amounts (Supplementary Fig. S32). Considering this observation, we studied the stability of DAB **23** in PBS at pH 7.4. In these conditions, the compound exhibited a half-life of 8h, corroborating

the observed hydrolysis of **24** (Supplementary Fig. S19). This slight instability is likely related to the presence of the ester function, which is known to be labile in aqueous conditions.

Considering the hydrolysis profile observed for DAB **23**, we evaluated if a self-immolative cascade directly promoted by the formation of the phenolic unit, would afford a more stable linker, as well as a more efficient release of the payload (Fig. 11). Therefore, starting from salicyladehyde, the 2-FPBA component was modified to include a benzyl alcohol *para* to the BA function, which then enabled the installation of SN-38, as shown in Fig. 11.

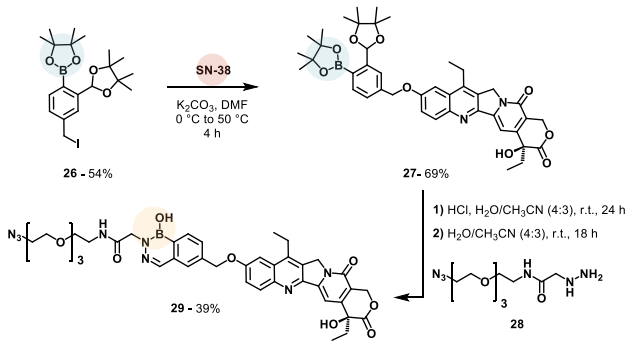

Figure 11. Synthetic route for the preparation of linker-payload **29**. Conditions for **27**: compound **26** (1.5 equiv), SN-38 (1 equiv), K_2CO_3 (1.5 equiv), DMF, 0°C-50°C, 4h, 69%. Conditions for **29**: HCl in H_2O/CH_3CN (4:3), 25°C, 24h; hydrazine **28** (6 equiv) in H_2O/CH_3CN (4:3), 25°C, 16h, 39%. DMF, N,N-dimethylformamide.

Once prepared, compound **27** was reacted with hydrazine **28** to afford DAB **29**. This hydrazine **28**, featuring a small polyethylene glycol, was selected to improve the aqueous solubility of the linker and to enable its installation on the biomolecule surface by a strain-promoted azide-alkyne cycloaddition (SPAAC) reaction. Once prepared, DAB **29** was tested for its stability in PBS pH 7.4 at 25°C where it displayed a half-life of over 100h (Fig.12a). Moreover, a similar stability was observed for this compound in human plasma (Fig.12b). Nonetheless, by adding H_2O_2 to **29** in PBS at pH 7.4, the diazaborine was readily oxidized (half-life 8.1 h) and released the SN-38 drug (Fig. 12c-d).

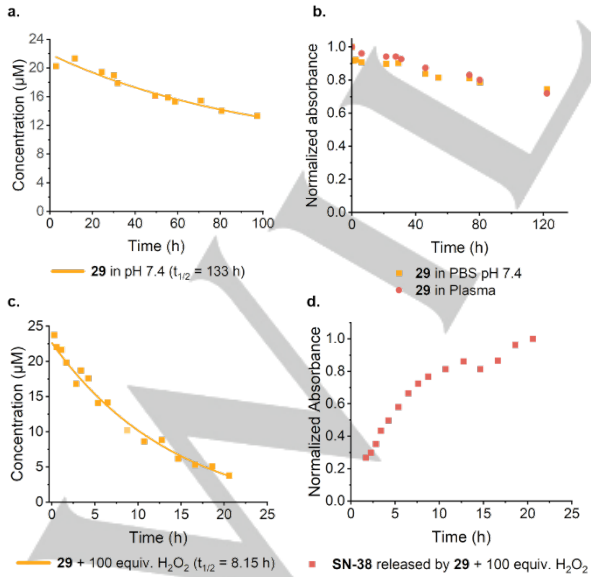

Figure 12. DAB **29** stability at different conditions analysed by HPLC. **(a)** DAB **29** stability in PBS/DMSO pH 7.4 at 25°C **(b)** DAB **29** stability in plasma at 25°C (compared with PBS pH 7.4 using the same analytical procedure); **(c)** Oxidation profile profile of DAB **29** oxidation in the presence of 100 equiv H_2O_2 (disappearance of the starting material) in PBS/DMSO pH 7.4 at 25°C; **(d)** SN-38 release profile during DAB **29** oxidation in the presence of 100 equiv H_2O_2 in PBS/DMSO pH 7.4. at 25°C. HPLC-MS traces of DAB **29** oxidation are presented as Supplementary Information (Fig. S26-28).

Then, we studied the conjugation of DAB **29** to the laminin fragment. To this end, a commercially available maleimide-cyclooctyne was used to functionalize the peptide and to react with DAB **29** by a SPAAC reaction to generate bioconjugate **Laminin-DAB31-SN-38** (Fig. 13). This reaction effectively generated the expected bioconjugate **31**, thereby a similar methodology was employed to construct a functional ADC against cancer cells.

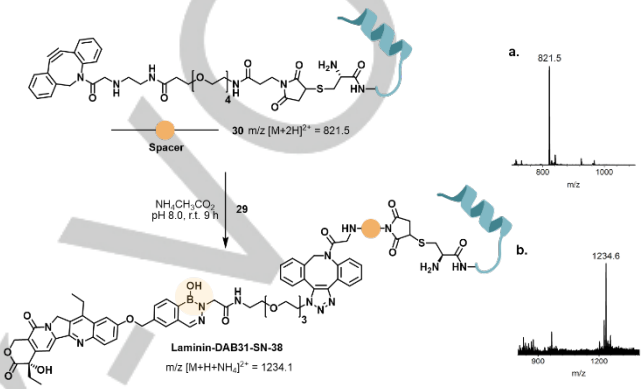

Figure 13. Reaction of DAB **29** in DMSO (2 mM) with laminin in ammonium acetate solution (10 µM, 20 mM, pH 8) at room temperature, after adding commercially available maleimide-PEG-cyclooctyne. **(a)** ESI-MS spectrum after the reaction of laminin with maleimide-PEG-cyclooctyne; **(b)** ESI-MS spectrum after the addition of compound **29**.

Recently, we initiated a program to develop an antibody fragment that selectively targets B-cell lymphoma cells and has the ability to internalize. This antibody scaffold consists on a rabbit derived VL single-domain antibody that exhibits a free cysteine at position 82 and can be explored to develop antibody-drug conjugates (ADC). This antibody scaffold was therefore modified with the maleimide-cyclooctyne cross linker and converted to the homogenous targeting drug conjugate **31**, **VL-DAB31-SN-38**, using the DAB **29** linker (Fig. 14).

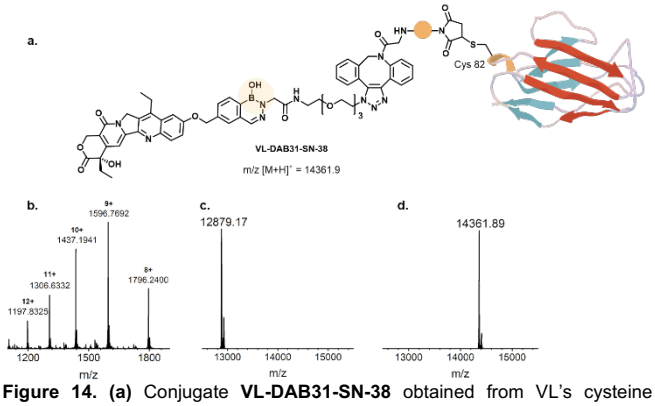

Figure 14. (a) Conjugate **VL-DAB31-SN-38** obtained from VL's cysteine modification with commercially available cyclooctyne **30**, followed by a SPAAC with DAB **29** (more details in the Supporting Info). **(b)** HRMS spectrum of conjugate **VL-DAB31-SN-38**; **(c)** Deconvoluted HRMS spectrum of VL (Mass: 12879.2 Da); **(d)** Deconvoluted HRMS spectrum of conjugate **VL-DAB31-SN-38** (14361.9 Da). Mass spectral deconvolution was performed using Zscore algorithm in MagTran1.03 software.[34]

Once prepared, this ADC was tested in the canine B-cell lymphoma CLBL-1 cell line and Jurkat cell line. The VL antibody was developed to target canine B-cell lymphomas and does not

recognize the human T lymphocyte Jurkat cell line. Therefore, this cell line was used as a control. The conjugate **VL-DAB31-SN-38** revealed to be highly cytotoxic toward the CLBL-1 cancer cell line with an IC_{50} value of 54.1 nM (Fig. 15a). In contrast, the unconjugated VL did not show cytotoxicity under the same conditions. Additionally, both the conjugate **VL-DAB31-SN-38** and the unconjugated VL, did not present cytotoxic activity against the Jurkat control cell line (Fig. 15b). The free SN-38 drug presented a potent and similar cytotoxicity activity in both the targeted cancer and control cell line (IC_{50} value of 4.67 nM and 10.6 nM respectively). To further characterize the mechanism of action of **VL-DAB31-SN-38**, we have conducted control experiments for linker DAB-PEG-N_3 and DAB **29** (SN38-DAB-PEG-N_3) in both cell lines (Figure S41). Moreover, a cellular ROS quantification assay was conducted on the CLBL-1 and Jurkat cell lines. This assay demonstrated that the CLBL-1 and Jurkat cell lines presented similar cellular ROS levels (Figure S42). Altogether, these results indicate that the **VL-DAB31-SN-38** exerts its cytotoxic activity due to the ADC internalization and SN-38 release under ROS-responsive cleavage.

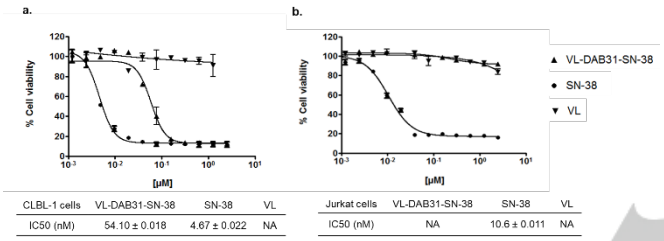

CLBL-1 cells	VL-DAB31-SN-38	SN-38	VL
IC50 (nM)	54.10 ± 0.018	4.67 ± 0.022	NA

Jurkat cells	VL-DAB31-SN-38	SN-38	VL
IC50 (nM)	NA	10.6 ± 0.011	NA

Figure 15. Cytotoxicity of conjugate **VL-DAB31-SN-38**. **(a)** Cytotoxic effect of conjugate **VL-DAB31-SN-38** on the CLBL-1 cell line. CLBL-1 cells (6×10^4) were subjected to the indicated concentrations of **VL-DAB31-SN-38**, SN-38 and VL. After 48 h treatment, cell viability and proliferation were evaluated with WST-1 reagent. Two replicate wells were utilized to determine each data point and three independent experiments were carried out in different days. Best-fit IC_{50} values of each compound were calculated using the log (inhibitor) vs response (variable slope) function; **(b)** Viability assay for conjugate **VL-DAB31-SN-38** on the Jurkat cell line (incubation time of 48 h).

Conclusion

In summary, here we presented an innovative technology to synthesize ROS-responsive ADCs based on DABs. The high stability of DAB **2** in buffer (over 14 days at pH 4.5, 7.4 and 9; plasma) and in plasma (over 5 days), together with the ability to be oxidized in the presence of H_2O_2 (0.422 and 0.103$M^{-1}S^{-1}$ with 100 and 10 equiv of H_2O_2 respectively) made this scaffold a very useful tool to prepare well-defined ROS-responsive ADCs. A detailed DFT study was performed to elucidate the mechanism of DAB **2** oxidation in the presence of H_2O_2, which revealed a similar pathway to the known oxidation of aromatic boronic acids with H_2O_2. Once established the high stability and ROS responsiveness of DABs, these scaffolds were applied in the synthesis of self-immolative linkers to release the cytotoxic payload SN-38. The linker was equipped with a maleimide that was used in the site-selective functionalization of a VL antibody. The obtained ADC **VL-DAB31-SN-38** presented a high selectivity and potency (IC_{50} = 54.1 nM) against B-cell lymphoma CLBL-1 cell line.

ROS is essential to sustain the biochemical alterations required for the initiation, promotion and progression of cancer, but is also a distinctive feature of many other important diseases (e.g neurodegeneration and inflammation), and until now, the development of ROS-responsive ADCs for these conditions has been limited by the existence of stable linkers that can effectively respond to ROS. The developed DABs oxidation technology is expected to overcome these limitations, and support the discovery of the next generation of stimuli-responsive ADCs.

Acknowledgements

The authors acknowledge the financial support from Fundação para a Ciência e a Tecnologia (FCT), Ministério da Ciência e da Tecnologia, Portugal (SFRH/BD/90514/2012 PD/BD/128239/2016, PD/BD/143124/2019, SFRH/BPD/102296/2014, iMed.ULisboa UIDB/04138/2020; SAICTPAC/0019/2015, PTDC/QUI-QOR/29967/2017, PTDC/BTM-SAL/32085/2017); LISBOA-01-0145-FEDER-029967. (LFV) Centro de Química Estrutural acknowledges the financial support of FCT (UIDB/00100/2020).

Conflict of Interest: J. P. M. António, J. I. Carvalho and Pedro M. P. Gois are inventors of portuguese provisional patent PPP11728 (Application number: 20211000023853). Patent rights granted to Technophage SA and Faculdade de Farmácia da Universidade de Lisboa. Frederico Aires-da-Silva, Joana N.R. Dias, Ana S. André, Sandra I. Aguiar, Soraia Oliveira, Luís Tavares are inventors of portuguese provisional patent filed on 13-09-2021 entitled Rabbit derived single-domain antibodies as promising scaffolds for the development of highly specific and potent antibody drug conjugates. The authors have no other relevant affiliations or financial involvement with any organization or entity with a financial interest in or financial conflict with the subject matter or materials discussed in the manuscript apart.

Keywords: Antibody-drug conjugate • Boronic acids, Diazaborines • Oxidative stress • Cleavable linkers • ROS.

[1] C. M. Mckertish, V. Kayser, *Biomedicines* **2021**, *9*, 872.

[2] S. J. Walsh, J. D. Bargh, F. M. Dannheim, A. R. Hanby, H. Seki, A. J. Counsell, X. Ou, E. Fowler, N. Ashman, Y. Takada, A. Isidro-Llobet, J. S. Parker, J. S. Carroll, D. R. Spring, *Chem. Soc. Rev.* **2021**, *50*, 1305–1353.

[3] J. D. Bargh, A. Isidro-Llobet, J. S. Parker, D. R. Spring, *Chem. Soc. Rev.* **2019**, *48*, 4361–4374.

[4] S. S. Sabharwal, P. T. Schumacker, *Nat. Rev. Cancer* **2014**, *14*, 709–721.

[5] G. Y. Liou, P. Storz, *Reactive Oxygen Species in Cancer*, **2010**.

[6] C. R. Reczek, N. S. Chandel, *Annu. Rev. Cancer Biol.* **2017**, *1*, 79–98.

[7] A. Bansal, M. C. Simon, *J. Cell Biol.* **2018**, *217*, 2291–2298.

[8] H. Lv, C. Zhen, J. Liu, P. Yang, L. Hu, P. Shang, *Oxid. Med. Cell. Longev.* **2019**, *2019*, 1–16.

[9] C. Gorrini, I. S. Harris, T. W. Mak, *Nat. Rev. Drug Discov.* **2013**, *12*, 931–947.

[10] J. Liang, B. Liu, *Bioeng. Transl. Med.* **2016**, *1*, 239–251.

[11] X. Xu, P. E. Saw, W. Tao, Y. Li, X. Ji, S. Bhasin, Y. Liu, D. Ayyash, J. Rasmussen, M. Huo, J. Shi, O. C. Farokhzad, *Adv. Mater.* **2017**, *29*, 1–6.

[12] Z. Dong, Z. Yang, Y. Hao, L. Feng, *Nanoscale* **2019**, *11*, 16164–

16186.

[13] P. Schmidt, C. Stress, D. Gillingham, *Chem. Sci.* **2015**, *6*, 3329–3333.

[14] E. J. Kim, S. Bhuniya, H. Lee, H. M. Kim, C. Cheong, S. Maiti, K. S. Hong, J. S. Kim, *J. Am. Chem. Soc.* **2014**, *136*, 13888–13894.

[15] J. P. M. António, R. Russo, C. P. Carvalho, P. M. S. D. Cal, P. M. P. Gois, *Chem. Soc. Rev.* **2019**, *48*, 3513–3536.

[16] A. Stubelius, S. Lee, A. Almutairi, *Acc. Chem. Res.* **2019**, *52*, 3108–3119.

[17] G. Högenauer, M. Woisetschläger, *Nature* **1981**, *293*, 662–664.

[18] M. A. Grassberger, F. Turnowsky, J. Hildebrandt, *J. Med. Chem.* **1984**, *27*, 947–953.

[19] C. Baldock, J. B. Rafferty, S. E. Sedelnikova, P. J. Baker, A. R. Stuitje, A. R. Slabas, T. R. Hawkes, D. W. Rice, *Science (80-.).* **1996**, *274*, 2107–2110.

[20] C. Baldock, G. J. De Boer, J. B. Rafferty, A. R. Stuitje, D. W. Rice, *Biochem. Pharmacol.* **1998**, *55*, 1541–1550.

[21] A. Bandyopadhyay, S. Cambray, J. Gao, *J. Am. Chem. Soc.* **2017**, *139*, 871–878.

[22] T. I. Chio, H. Gu, K. Mukherjee, L. N. Tumey, S. L. Bane, *Bioconjug. Chem.* **2019**, *30*, 1554–1564.

[23] J. P. M. António, L. M. Gonçalves, R. C. Guedes, R. Moreira, P. M. P. Gois, *ACS Omega* **2018**, *3*, 7418–7423.

[24] M. Z. H. Kazmi, J. P. G. Rygus, H. T. Ang, M. Paladino, M. A. Johnson, M. J. Ferguson, D. G. Hall, *J. Am. Chem. Soc.* **2021**, jacs.1c02462.

[25] O. Dilek, Z. Lei, K. Mukherjee, S. Bane, *Chem. Commun.* **2015**, *51*, 16992–16995.

[26] D. Kanichar, L. Roppiyakuda, E. Kosmowska, M. A. Faust, K. P. Tran, F. Chow, E. Buglo, M. P. Groziak, E. A. Sarina, M. M. Olmstead, I. Silva, H. H. Xu, *Chem. Biodivers.* **2014**, *11*, 1381–1397.

[27] R. G. Parr, W. Yang, *Density Functional Theory of Atoms and Molecules*, **1989**.

[28] H. G. Kuivila, A. G. Armour, *J. Am. Chem. Soc.* **1957**, *79*, 5659–5662.

[29] H. G. Kuivila, T. C. Muller, *J. Am. Chem. Soc.* **1962**, *84*, 377–382.

[30] D. M. Goldenberg, R. M. Sharkey, *Expert Opin. Biol. Ther.* **2020**, *20*, 871–885.

[31] A. Nagayama, N. Vidula, L. Ellisen, A. Bardia, *Ther. Adv. Med. Oncol.* **2020**, *12*, 175883592091598.

[32] S. Lopez, E. Perrone, S. Bellone, E. Bonazzoli, B. Zeybek, C. Han, J. Tymon-Rosario, G. Altwerger, G. Menderes, A. Bianchi, L. Zammataro, A. Manzano, P. Manara, E. Ratner, D.-A. Silasi, G. S. Huang, M. Azodi, P. E. Schwartz, F. Raspagliesi, R. Angioli, N. Buza, P. Hui, H. M. Bond, A. D. Santin, *Oncotarget* **2020**, *11*, 560–570.

[33] D. M. Goldenberg, T. M. Cardillo, S. V. Govindan, E. A. Rossi, R. M. Sharkey, *Oncotarget* **2020**, *11*, 942–942.

[34] Z. Zhang, A. G. Marshall, *J. Am. Soc. Mass Spectrom.* **1998**, *9*, 225–233.

Entry for the Table of Contents

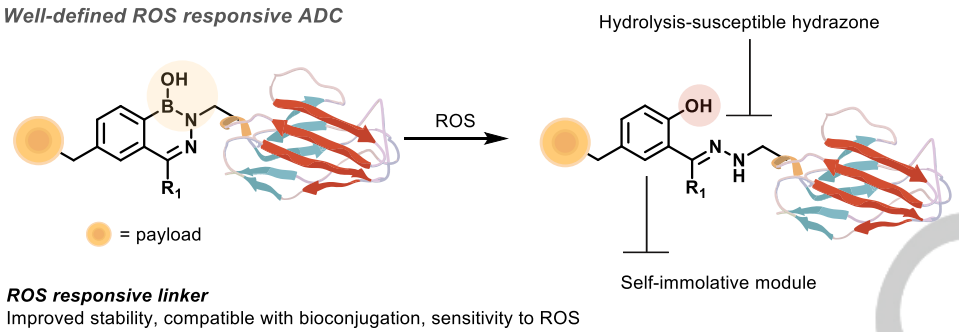

ROS responsive linker
Improved stability, compatible with bioconjugation, sensitivity to ROS

Oxidation of physiologically stable diazaborines in the presence of reactive oxygen species (ROS) enable the construction of ROS responsive antibody drug conjugates.